

Article

Composition Engineering of $(\text{Lu,Gd,Tb})_3(\text{Al,Ga})_5\text{O}_{12}:\text{Ce}$ Film/ $\text{Gd}_3(\text{Al,Ga})_5\text{O}_{12}:\text{Ce}$ Substrate Scintillators

Oleg Sidletskiy ^{1,2,*}, Vitalii Gorbenko ¹, Tetiana Zorenko ¹, Yurii Syrotych ¹ , Sandra Witkiwicz-Lukaszek ¹, Jiri A. Mares ³, Romana Kucerkova ³, Martin Nikl ³ , Iaroslav Gerasymov ², Daniil Kurtsev ², Alexander Fedorov ⁴ and Yuriy Zorenko ^{1,5} 

¹ Institute of Physics, Kazimierz Wielki University in Bydgoszcz, Powstańców Wielkopolskich Str., 2, 85090 Bydgoszcz, Poland

² Institute for Scintillation Materials, National Academy of Sciences of Ukraine, Nauky Ave., 60, 61072 Kharkiv, Ukraine

³ Institute of Physics, Academy of Sciences of Czech Republic, Cukrovarnicka Str., 10, 16200 Prague, Czech Republic

⁴ State Scientific Institution "Institute for Single Crystals" of National Academy of Sciences of Ukraine, Nauky Ave., 60, 61072 Kharkiv, Ukraine

⁵ Oncology Center, Medical Physics Department, Romanowskiej Str., 2, 85796 Bydgoszcz, Poland

* Correspondence: sidletskiy@isma.kharkov.ua



Citation: Sidletskiy, O.; Gorbenko, V.; Zorenko, T.; Syrotych, Y.; Witkiwicz-Lukaszek, S.; Mares, J.A.; Kucerkova, R.; Nikl, M.; Gerasymov, I.; Kurtsev, D.; et al. Composition Engineering of $(\text{Lu,Gd,Tb})_3(\text{Al,Ga})_5\text{O}_{12}:\text{Ce}$ Film/ $\text{Gd}_3(\text{Al,Ga})_5\text{O}_{12}:\text{Ce}$ Substrate Scintillators. *Crystals* **2022**, *12*, 1366. <https://doi.org/10.3390/cryst12101366>

Academic Editor: Hong Joo Kim

Received: 13 September 2022

Accepted: 24 September 2022

Published: 27 September 2022

Publisher's Note: MDPI stays neutral with regard to jurisdictional claims in published maps and institutional affiliations.



Copyright: © 2022 by the authors. Licensee MDPI, Basel, Switzerland. This article is an open access article distributed under the terms and conditions of the Creative Commons Attribution (CC BY) license (<https://creativecommons.org/licenses/by/4.0/>).

Abstract: The paper addresses the development of composite scintillation materials providing simultaneous real-time monitoring of different types of ionizing radiation (α -, β -particles, γ -rays) in mixed fluxes of particles and quanta. The detectors are based on composite heavy oxide scintillators consisting of a thin single-crystalline film and a bulk single-crystal substrate. The film and substrate respond to certain types of ionizing particles, forming together an all-in-one composite scintillator capable of distinguishing the type of radiation through the different time characteristics of the scintillation response. Here, we report the structure, composition, and scintillation properties under different ionizing radiations of $(\text{Lu,Gd,Tb})_3(\text{Al,Ga})_5\text{O}_{12}:\text{Ce}$ films deposited using liquid phase epitaxy onto $\text{Gd}_3(\text{Al}_{1-x}\text{Ga}_x)_5\text{O}_{12}:\text{Ce}$ (GAGG:Ce) single-crystal substrates. The most promising compositions with the highest light yields and the largest differences in scintillation decay timing under irradiation with α -, β -particles, and γ -rays were selected. Such detectors are promising for environmental security purposes, medical tomography, and other radiation detection applications.

Keywords: scintillators; garnets; radiation detectors; bulk crystal; thin single-crystalline films; liquid phase epitaxy; ionization radiation

1. Introduction

Today, radiation detectors (both scintillation and semiconductor) are typically designed for the registration of a certain type of ionizing radiation. In this way, γ -rays, X-rays, high-energy protons, electrons, etc. are detected with high efficiency by inorganic bulk materials with a high atomic number (density) capable of attenuating these quanta and particles and converting them into UV or visible light photons (in scintillators), or directly into an electric current (in semiconductors). However, to distinguish neutrons or charged α - or β -particles with short attenuation lengths from γ - and X-rays, the detector thickness should be as small as possible and/or the material density should be as low as possible to minimize the absorption of high-energy particles contained in mixed fluxes. For example, detectors based on plastic scintillators [1,2] designed for neutron–gamma discrimination are bulky due to their low density. Meanwhile, in real conditions of environmental radiation monitoring, radiation fluxes consist of different types of particles with different impacts on human health and the environment. As an alternative, compact composite multilayer detectors based on heavy oxide scintillators may enable simultaneous identification of different

types of particles by choosing the proper thickness and composition of a single-crystalline substrate and thin single-crystalline film(s) deposited onto the mentioned substrate [3–6]. In the proposed solution, each layer in a multilayer detector is sensitive to a certain type of ionizing radiation. The scintillation response from each layer is distinguished by its decay time and/or the wavelength of luminescence band. The optimal time discrimination is achieved by activation of the layers with dopants that have different luminescence decay times (Pr^{3+} in the range of 10–30 ns, Ce^{3+} in the range of 20–70 ns, Sc^{3+} in the range of hundreds of ns, etc.). Discrimination by luminescence wavelength is also possible due to the fact that the mentioned activators possess characteristic luminescence bands. At the same time, each subsequent layer has to be transparent to luminescence from the previous layer(s) in order to collect all emitted light by a photodetector. Therefore, the detection of certain types of ionizing radiation is possible by distinguishing the time profiles (scintillation decay times) and/or luminescence bands of scintillation responses related to each type of ionizing radiation.

The concept of composite scintillators (CS) for distinguishing different types of high-energy particles in mixed fluxes has been developed in recent years (see [7] and citations therein). The idea comprises the simultaneous registration of high-penetrating γ - or X-rays by a bulk crystalline substrate, and low-penetrating α - or β -particles by a single-crystalline film deposited onto the substrate. Herein, the film and substrate must possess different luminescence decay times and/or emission wavelengths due to doping with different activators, or different host composition of the substrate and film. Consequently, the best discrimination between the luminescence from a substrate and film is achieved at the largest difference between scintillation decay times of substrate and film materials. At the same time, the scintillation light output should be as high as possible to clearly discriminate the signals in cases of low irradiation dose.

The main focus in the development of composite scintillators is on garnet-type compounds such as LuAG:A^{3+} ($A = \text{Ce}, \text{Pr}, \text{Sc}$) [8–11], $(\text{Lu,Gd,Tb})\text{AG:Ce}$ [12–14], and $\text{Tb}_3\text{Al}_5\text{O}_{12}:\text{Ce}$ [15] due to their high light yield and quite fast scintillation decay, chemical stability, easy tuning of energy structure by optimization of host composition, and relatively easy production of films with cubic space symmetry using the liquid phase epitaxy (LPE) method. Among such garnets, the highest light yield was registered in GAGG:Ce and other Al-Ga-substituted bulk crystals [16–19] and single-crystalline films [13,20]. While substrate compositions are limited to Y-Lu-Gd-substituted systems due to the inability to produce bulk crystals of Tb-based garnets from melt because of incongruent melting, the single-crystalline films of $\text{Tb}_3\text{Al}_5\text{O}_{12}$ and other Tb-containing mixed compositions can be grown from melt solutions [12,15], providing more room for engineering of garnet compositions.

Fabrication of such films became possible due to the combination of advanced technologies of single-crystal growth and single-crystalline film deposition. LPE is an efficient method for preparation of composite substrate-film scintillators with a prescribed thickness and composition. Single-crystalline films based on garnet [8–15], orthosilicate [21–24], perovskite [25–28], and other complex oxide compounds have been fabricated successfully from PbO or Bi_2O_3 fluxes, and most promising compositions have been selected. Nowadays, the LPE method offers the possibility of creating “phoswich-type” (phosphor sandwich) composite scintillators based on epitaxial crystalline structures for registration of low-penetrating α - and β -particles, and bulk single-crystal substrates for registration of high-penetrating radiation (X- or γ -rays). The LPE method for composite scintillator production also enables adjustment of the thickness of the film scintillators according to the penetration depth of registered particles. Specifically, the thickness providing complete absorption of α -particles of ^{239}Pu and ^{241}Am radioisotopes typically equals 12–15 μm [7]. Therefore, the thickness of LPE-grown scintillation thin films usually does not exceed 15–50 μm .

This paper addresses the growth of $\text{RE}_3\text{Al}_{5-x}\text{Ga}_x\text{O}_{12}:\text{Ce}$ ($R = \text{Lu}, \text{Gd}, \text{Tb}$) single-crystalline films deposited using the LPE method onto $\text{Gd}_3\text{Al}_{5-x}\text{Ga}_x\text{O}_{12}:\text{Ce}$ (GAGG:Ce)

substrates with $x = 2.5$ and describes testing of their structure, composition, and optical and scintillation properties under α -, β -, and γ -irradiation in comparison with previously studied composite scintillators [8–10,12–14]. Misfits between substrate and film lattice parameters were determined for some composite scintillators based on X-ray diffraction and rocking curve measurements. Simultaneously, the segregation coefficients of the host and activator cations were calculated. A high flexibility of host cation composition in the epitaxial structures provides the possibility of precise tuning of scintillation performance of composite scintillators. Further recommendations are elaborated to improve the parameters of radiation detectors based on the developed scintillators.

2. Materials and Methods

2.1. Fabrication of Substrates

Substrates with the composition of $\text{Gd}_3\text{Al}_{5-x}\text{Ga}_x\text{O}_{12}:\text{Ce}$ ($x = 2.5$) were fabricated from Czochralski-grown crystals produced by the Institute for Scintillation Materials (Kharkiv, Ukraine). Typical crystal size was 30 mm diameter and 30–100 mm length. The crystals were annealed at 1250–1300 °C in an air atmosphere to eliminate color centers related to oxygen vacancies. The substrates were cut using a diamond wire saw and ground at ISMA, then chemically–mechanically polished in a SiO_2 slurry at CIA Karat, Lviv, Ukraine. A typical substrate cross-section was $5 \times 5 \text{ mm}^2$ and had a thickness of 1 mm.

2.2. Film Deposition via LPE Method

Composite scintillators based on garnet crystals and films were grown using the LPE method in the Epitaxy Laboratory of the Chair for Optoelectronic Materials in the Institute of Physics of Kazimierz Wielki University (UKW) in Bydgoszcz, Poland.

To get a high-quality multilayer scintillator, the misfit between lattice parameters of the single-crystalline substrate and film must not exceed 0.5–1% [29]. The single-crystalline films (SCF) were grown by the LPE method both from BaO and PbO fluxes, the basic features of which are described elsewhere [7,29,30]. In total, over 40 samples of composite scintillators based on GAGG:Ce substrates and $(\text{Lu,Gd,Tb})_3\text{Al}_{5-x}\text{Ga}_x\text{O}_{12}:\text{Ce}$ films with thicknesses within the 5–125 μm range were prepared (Figure 1). The nominal film compositions are presented in Table 1. The Ce concentration in the melt solution was 10 at% relative to the total concentration of the lanthanide cations.

Table 1. Nominal contents of rare earth cations in the studied films grown from different fluxes.

BaO Flux	PbO Flux
$\text{Gd}_3\text{Al}_{1.5}\text{Ga}_{3.5}\text{O}_{12}$ $\text{Gd}_3\text{Al}_3\text{Ga}_2\text{O}_{12}$ $\text{Gd}_3\text{AlGa}_4\text{O}_{12}$	$\text{Gd}_3\text{Al}_3\text{Ga}_2\text{O}_{12}$ $\text{Gd}_3\text{Al}_2\text{Ga}_3\text{O}_{12}$
$\text{Tb}_{1.5}\text{Gd}_{1.5}\text{Al}_{1.5}\text{Ga}_{3.5}\text{O}_{12}$ $\text{Tb}_{1.5}\text{Gd}_{1.5}\text{Al}_2\text{Ga}_3\text{O}_{12}$ $\text{Tb}_{1.5}\text{Gd}_{1.5}\text{Al}_{3.25}\text{Ga}_{1.75}\text{O}_{12}$	$\text{Tb}_3\text{Al}_5\text{O}_{12}$ $\text{Tb}_2\text{GdAl}_{1.5}\text{Ga}_{3.5}\text{O}_{12}$ $\text{Tb}_3\text{Al}_{2.25}\text{Ga}_{2.75}\text{O}_{12}$ $\text{Tb}_3\text{Al}_{1.5}\text{Ga}_{3.5}\text{O}_{12}$
$\text{Lu}_{1.5}\text{Gd}_{1.5}\text{Al}_2\text{Ga}_3\text{O}_{12}$ $\text{Lu}_{1.5}\text{Gd}_{1.5}\text{Al}_3\text{Ga}_2\text{O}_{12}$	$\text{Lu}_1\text{Gd}_2\text{Al}_1\text{Ga}_4\text{O}_{12}$ $\text{Lu}_{1.5}\text{Gd}_{1.5}\text{Al}_{1.5}\text{Ga}_{3.5}\text{O}_{12}$ $\text{Lu}_1\text{Gd}_2\text{Al}_{1.5}\text{Ga}_{3.5}\text{O}_{12}$

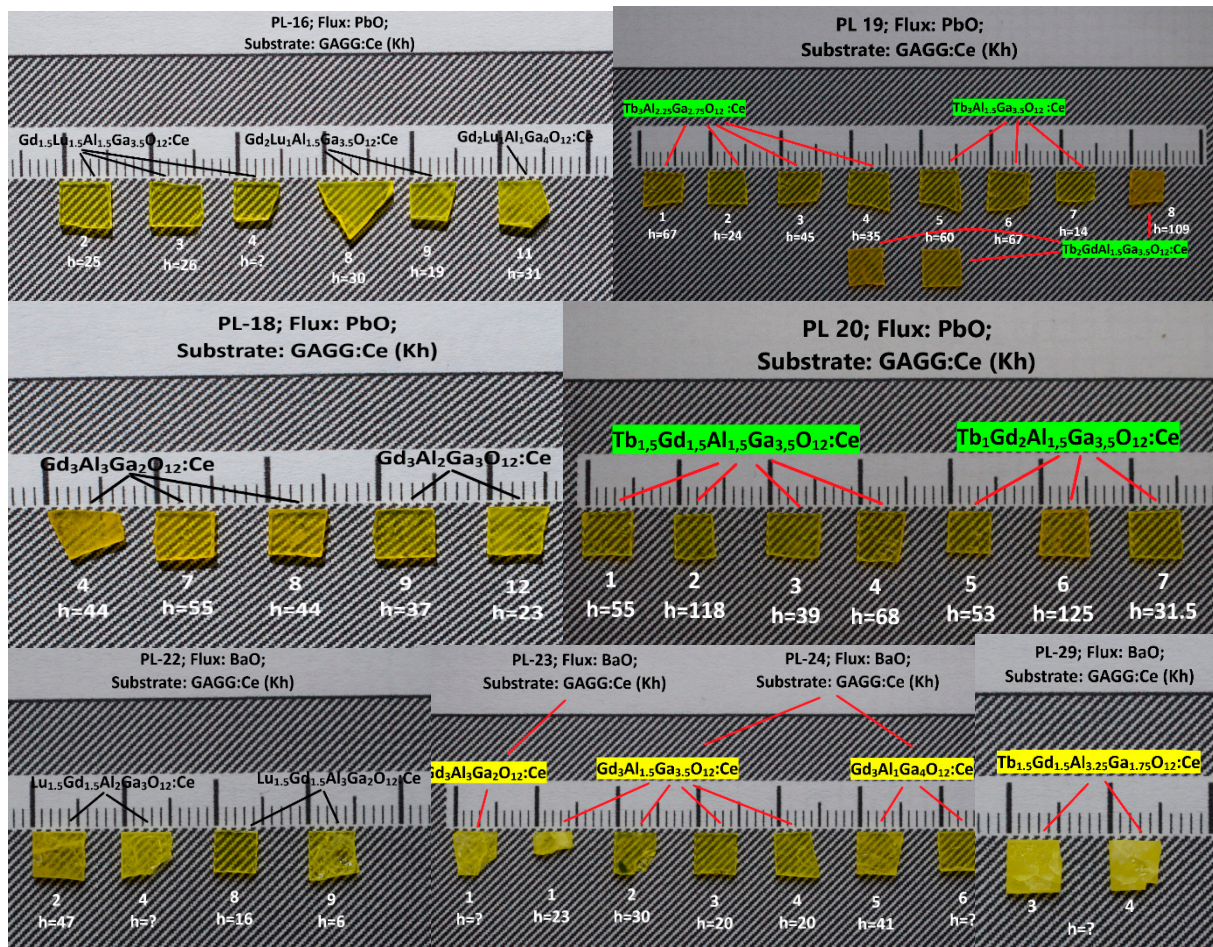


Figure 1. Multicomponent garnet composite scintillators fabricated in this work and their thicknesses in μm .

2.3. Determination of Optical and Scintillation Parameters

The absorption spectra were registered using a Jasco 760 UV–vis spectrometer in the 200–1100 nm range. The cathodoluminescence (CL) spectra were registered at room temperature (RT) using an e-beam in a SEM JEOL JSM-820 electron microscope equipped with a Stellar Net spectrometer and a TE-cooled CCD detector working in the 200–925 nm range.

Express control of the scintillation light yield and scintillation decay kinetic of the film parts of composite scintillators and substrates was performed using a set-up consisting of a Hamamatsu H6521 photomultiplier, homemade multichannel analyzer working with the shaping time of 12 μs , and a Tektronix TDS3052 digital oscilloscope under excitation by α -particles from a ^{239}Pu (5.15 MeV) source. The pulse-height spectra (PHS) were compared with the standard YAG:Ce SCF sample with a photoelectron yield of 360 phels/MeV and a LY of 2.65 photons/keV. Herein, α -particles from a ^{239}Pu source (energy of 5.15 MeV) excited only the epitaxial layers of film samples (not their substrates), because α -particle penetration depth in the studied materials was approximately 12–15 μm [7].

Next, investigations of the scintillation responses of the composite scintillators under study and reference substrates were performed, also at the Institute of Physics of the Czech Academy of Sciences in Prague (FZU), using a set-up consisting of a hybrid PMT (HPMT DEP PP0475B with a pre-amplifier), measuring electronics (Ortec 672 Spectroscopy Amplifier and 927 ASPEC MCA), and PC control. The PHS were measured using different shaping times in the 0.5–10 μs range under excitation by α -particles from ^{241}Am (energy of 5.49 MeV) and ^{239}Pu (5.15 MeV) sources, β -particles from a $^{90}\text{Sr} + ^{90}\text{Y}$ source (continuous

distribution of energies of average values 0.546 and 0.939 MeV for ^{90}Sr and ^{90}Y , respectively), and γ -rays from ^{137}Cs (an energy of 662 keV) radio-isotopes. N_{photo} photoelectron yield measurements of the selected samples were also performed under α -radiation of 4.8 MeV of ^{241}Am with a thin palladium foil (from a special source at CERN in Geneva) and under γ -radiation of 662 keV.

3. Results

3.1. Determination of Film Structure and Composition

The lattice parameters of the Lu-Gd-Tb-substituted films were smaller than those of the GAGG:Ce substrate due to the lower amounts of Gd atoms. Logically, the films with larger Ga and Gd contents possessed lower misfits (Figure 2a). Overall, the misfit between the GAGG:Ce substrate and film lattice parameters did not exceed 0.71%. The XRD rocking curves with a FWHM of 0.037–0.047° proved a very good structural quality of the yielded films (Figure 2b).

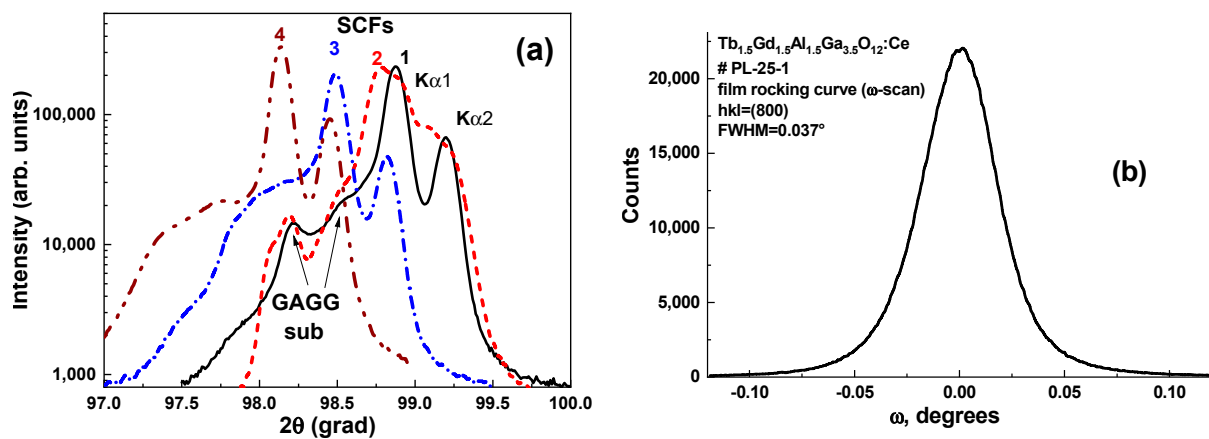


Figure 2. (a) XRD patterns of $(\text{Tb,Lu,Gd})_3(\text{Al,Ga})\text{O}_{12}:\text{Ce}$ SCFs with different nominal contents (1— $\text{Tb}_3\text{Al}_{2.25}\text{Ga}_{2.75}\text{O}_{12}:\text{Ce}$ SCF, 24 μm thickness, misfit $\Delta a = -0.49\%$; 2— $\text{Lu}_{1.5}\text{Gd}_{1.5}\text{Al}_3\text{Ga}_2\text{O}_{12}:\text{Ce}$ SCF, 6 μm , $\Delta a = -0.71\%$; 3— $\text{Tb}_2\text{GdAl}_{1.5}\text{Ga}_{3.5}\text{O}_{12}:\text{Ce}$ SCF, 35 μm , $\Delta a = -0.20\%$; 4— $\text{TbGd}_2\text{Al}_{1.5}\text{Ga}_{3.5}\text{O}_{12}:\text{Ce}$ SCF; 125 μm , $\Delta a = -0.54\%$); (b) X-ray rocking curve of $\text{Tb}_{1.5}\text{Gd}_{1.5}\text{Al}_{1.5}\text{Ga}_{3.5}\text{O}_{12}:\text{Ce}$ SCF, 6 μm .

Based on the results of the film composition measurements, the segregation coefficients of different cations were determined. Predictably, the segregation coefficients of RE atoms in dodecahedral positions of Lu-Gd-substituted garnet hosts were larger for smaller Lu (1.11–1.27) atoms in contrast to larger Gd atoms (0.83–0.95), in line with an earlier fundamental work on admixture segregation in garnet compounds [30]. It is important to note the larger Gd segregation coefficient at growth from BaO flux (0.95) as compared to that from PbO flux (0.83). As the difference between the ionic radii of Gd and Tb is very small, their segregation coefficients were quite similar among the Tb-Gd-substituted samples, in the range of 0.90–1.17 for Tb and 0.90–1.06 for Gd, independently of the flux type.

Regarding the segregation coefficients of Al/Ga occupying tetrahedral and octahedral positions, a large difference was observed between the samples grown from PbO and BaO fluxes (Figure 3). For the growth from PbO flux, the segregation coefficient of smaller Al atoms (1.50–1.81) was remarkably larger than that of larger Ga cations (0.62–0.78), which agrees well with results presented in [30].

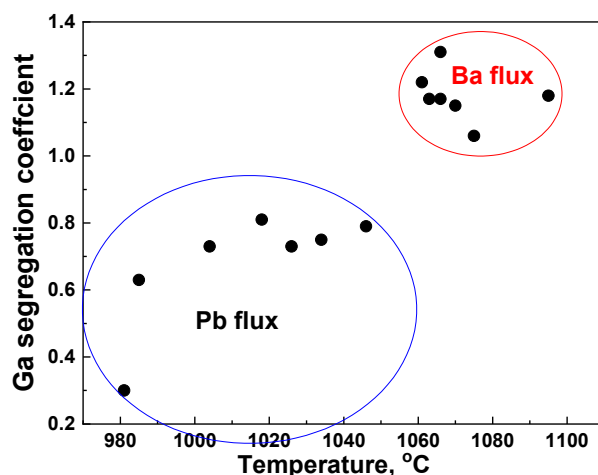


Figure 3. Ga segregation coefficients in $(\text{Tb,Al})_3(\text{Al,Ga})_5\text{O}_{12}:\text{Ce}$ SCFs deposited via the LPE method onto GAGG:Ce substrates, dependent on crystallization temperature.

However, the reciprocal situation was observed in the samples grown from BaO flux, where Al segregation coefficients were 0.49–0.82 in contrast to Ga segregation coefficients of 1.13–1.25 (Figure 3). This discrepancy may be attributed to a compensation of the lattice misfit between GAGG:Ce substrate with a larger lattice constant of 12.23 Å and smaller lattice constant of the films, which reached 0.71 %, as shown above. This misfit in the films grown from PbO flux was partially compensated by the incorporation of large Pb^{2+} atoms with an ionic radius of 1.29 Å into dodecahedral sites. For instance, the actual composition of the film with the $\text{Gd}_{1.5}\text{Lu}_{1.5}\text{Al}_{1.5}\text{Ga}_{3.5}\text{O}_{12}:\text{Ce}$ nominal composition was $\text{Gd}_{1.406}\text{Lu}_{1.521}\text{Pb}_{0.0011}\text{Ce}_{0.0057}\text{Ga}_{2.294}\text{Al}_{2.814}\text{O}_{12}$, whereas Ba was not detected in the films grown from the BaO flux within the available measurement precision. Preferential introduction of Ga with the ionic radii of 0.47 and 0.62 Å in the tetrahedral and octahedral sites, respectively, against the 0.39 and 0.53 Å for Al, contributed to minimization of the lattice misfit between the substrates and films. The same mechanism may explain the phenomenon mentioned above of a larger Gd segregation coefficient in films grown from BaO flux.

Furthermore, the LPE crystallization of films from BaO flux proceeded at a 50 °C higher temperature than the growth from PbO flux (Figure 3). Therefore, temperature changes may also cause a sharp increase in the Ga segregation coefficient, which is more sensitive to crystallization temperature variation [30]. The Ce segregation coefficients of 0.009–0.0028 were typical for growth via the low-temperature LPE method and tended to decrease in Gd- and Ga-rich compositions.

3.2. Primary Selection of Promising Compositions

First, we screened the compositions by their light yield and scintillation decay time under α -particle excitation. Films with a thickness of over 15 μm were selected to ensure that α -particles were completely absorbed into them.

Light output in dependence on nominal cationic composition (Figure 4a) reflects the tendency to increase with reducing Ga content and average radius of a rare earth (RE) ion, namely by increasing Lu or Tb contents in the solid solutions. Meanwhile, another spot with high light yields was located at a Ga content of 3.5 formula units (f. u.) (Figure 4c). Considering the Gd-Lu (Figure 4b) and Gd-Tb (Figure 4c) mixed compositions separately, one may note that the tendency to light yield increase with reducing Ga and increasing Lu(Tb) content was sustained in both compositions. Meanwhile, a very high light yield of up to 380 % relative to YAG:Ce was observed in Gd-Tb mixed compositions at a Ga content around 3.5 f. u. Note that we presumed that the light yield in Al-free samples, i.e., at Ga content of 5 f. u., was equal to zero, as has been reported by different groups for Ce-doped $\text{Y}_3\text{Ga}_5\text{O}_{12}$, $\text{Gd}_3\text{Ga}_5\text{O}_{12}$, and $\text{Lu}_3\text{Ga}_5\text{O}_{12}$ [17,18]. The data on light yield in GAGG:Ce films

crystallized into GAGG substrates were taken from [7]. Overall, the region with the highest light yields extended from Lu-containing samples at $x = 2-3$ to Gd-Tb-substituted samples at $x = 3.5-4$ (Figure 4a).

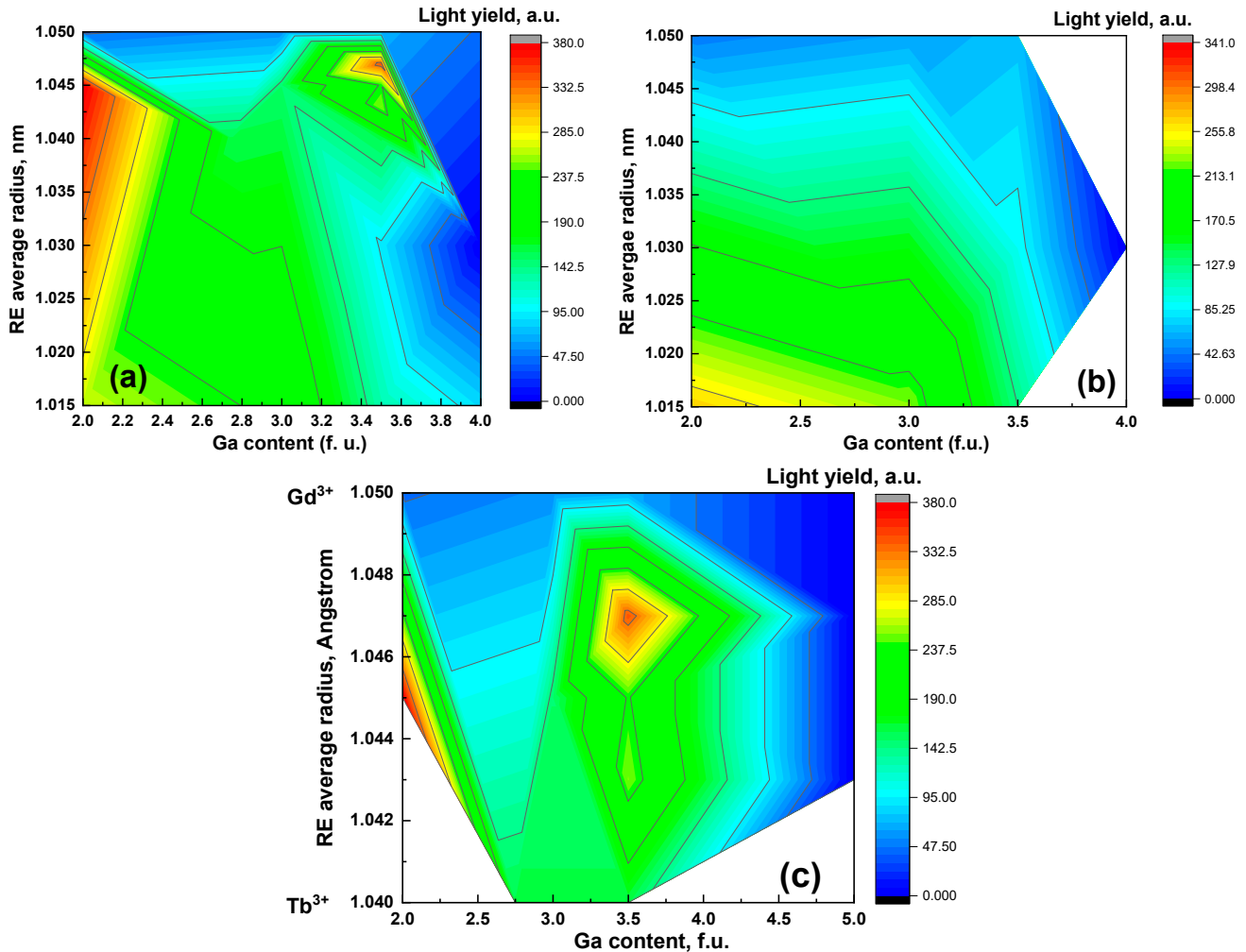


Figure 4. Light yield in $(\text{Gd,Lu,Tb})_3(\text{Al,Ga})_5\text{O}_{12}:\text{Ce}$ films on GAGG:Ce substrates in dependence on average ionic radius of the rare earth ion and Ga content in the films under α -particle excitation in (a) all the sample series, (b) Lu-Gd-substituted films, and (c) Gd-Tb-substituted films.

The scintillation decay times predictably decreased with Ga content (Figure 5), while there was a tendency to acceleration of scintillation decay with Lu and Tb addition. In general, the observed correlations were the result of the interplay between carrier trapping and energy transfer phenomena between Gd^{3+} and Tb^{3+} host cations and Ce^{3+} activator, as well as carrier trapping and thermal ionization of electrons from the $5d_1$ level of Ce^{3+} [31–35]. Furthermore, cationic composition (represented as an averaged ionic radius of Lu, Gd, and Tb cations in dodecahedral sites, as well Ga content in octahedral and tetrahedral sites, affected the crystal's field and location of carrier traps and Ce^{3+} levels in the bandgap.

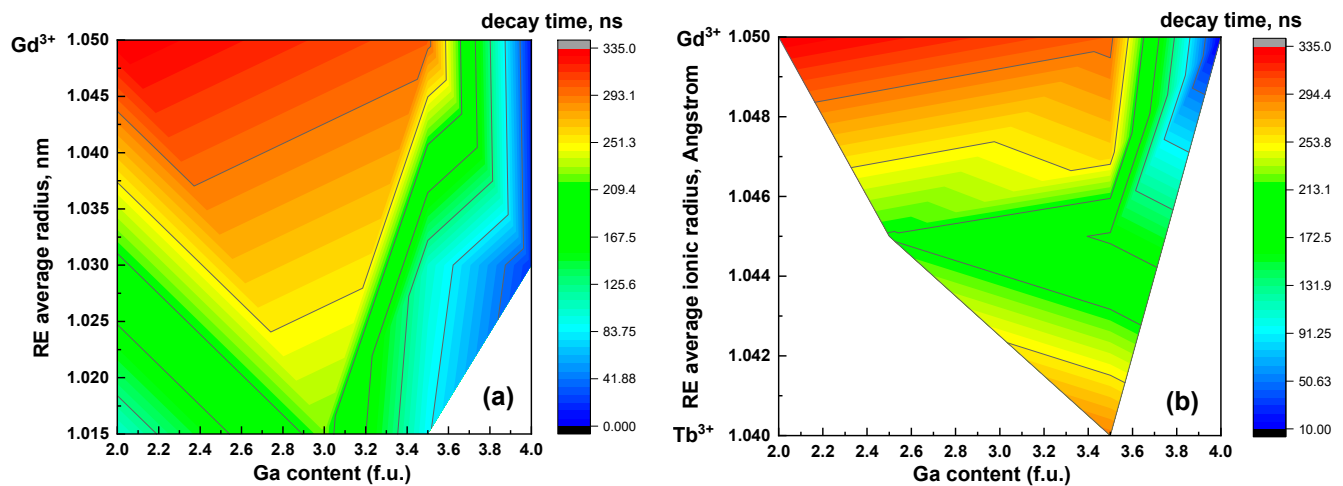


Figure 5. Scintillation decay time ($1/e$) in $(\text{Gd,Lu})_3(\text{Al,Ga})_5\text{O}_{12}:\text{Ce}$ (a) $(\text{Gd,Tb})_3(\text{Al,Ga})_5\text{O}_{12}:\text{Ce}$ (b) films in dependence on average ionic radius of the rare earth ion and Ga content in the films under α -particle excitation.

3.3. Characterization of Selected Composite Scintillators

Following the results of light yield and scintillation decay in $(\text{Gd,Lu,Tb})_3(\text{Al,Ga})_5\text{O}_{12}:\text{Ce}$ films deposited onto GAGG:Ce substrates (Figures 4 and 5), seven compositions with high light yields, four grown from PbO flux, and three grown from BaO flux, were selected for detailed characterization. The samples are listed in Table 2.

Table 2. List of the selected composite scintillators and their film thicknesses as used in detailed tests of scintillation performance.

Sample Number	Sample Composition	Used Flux	Sample Thickness, μm
Substrate	$\text{Gd}_3\text{Al}_2.5\text{Ga}_{2.5}\text{O}_{12}:\text{Ce}$ (GAGG:Ce)		1 mm
PL16-4	$\text{Gd}_{1.5}\text{Lu}_{1.5}\text{Al}_{1.5}\text{Ga}_{3.5}\text{O}_{12}:\text{Ce}/\text{GAGG}:\text{Ce}$	PbO	40
PL19-10	$\text{Tb}_2\text{GdAl}_{1.5}\text{Ga}_{3.5}\text{O}_{12}:\text{Ce}/\text{GAGG}:\text{Ce}$	PbO	33
PL20-3	$\text{Tb}_{1.5}\text{Gd}_{1.5}\text{Al}_{1.5}\text{Ga}_{3.5}\text{O}_{12}:\text{Ce}/\text{GAGG}:\text{Ce}$	PbO	39
PL20-7	$\text{Tb}_1\text{Gd}_2\text{Ga}_{3.5}\text{Al}_{1.5}\text{O}_{12}:\text{Ce}/\text{GAGG}:\text{Ce}$	PbO	31.5
PL22-8	$\text{Lu}_{1.5}\text{Gd}_{1.5}\text{Al}_3\text{Ga}_2\text{O}_{12}:\text{Ce}/\text{GAGG}:\text{Ce}$	BaO	16
PL25-3	$\text{Tb}_{1.5}\text{Gd}_{1.5}\text{Al}_{1.5}\text{Ga}_{3.5}\text{O}_{12}:\text{Ce}/\text{GAGG}:\text{Ce}$	BaO	42
PL25-10	$\text{Tb}_{1.5}\text{Gd}_{1.5}\text{Al}_2\text{Ga}_3\text{O}_{12}:\text{Ce}/\text{GAGG}:\text{Ce}$	BaO	63

Scintillation Parameters

Normalized CL luminescence spectra of film and substrate parts of composite scintillators were typical for Ce-doped garnets, with a wide band peaking in the 527–532 nm range corresponding to the $\text{Ce}^{3+} 5d-4f$ radiative transitions (Figure 6a,b). The emission spectra of Lu-containing film scintillators were predictably blue-shifted as compared with that of the GAGG:Ce substrate due to a lower crystal field strength in the dodecahedral positions of the garnet host [32,33]. The spectra of Tb-containing scintillators were modulated with several narrow bands around 490, 550, 580, and 620 nm (Figure 6b) corresponding to $5d-4f$ transitions of Tb^{3+} [36], indicating a competition between Tb^{3+} and Ce^{3+} luminescence centers. The highest intensity was registered in the Lu-Gd mixed samples in agreement with the data on light yield under α -particle irradiation (see Table 3). A negligible spectral intensity was noted in the UV band indicating an absence of defect-related luminescence in the LPE-grown film scintillators.

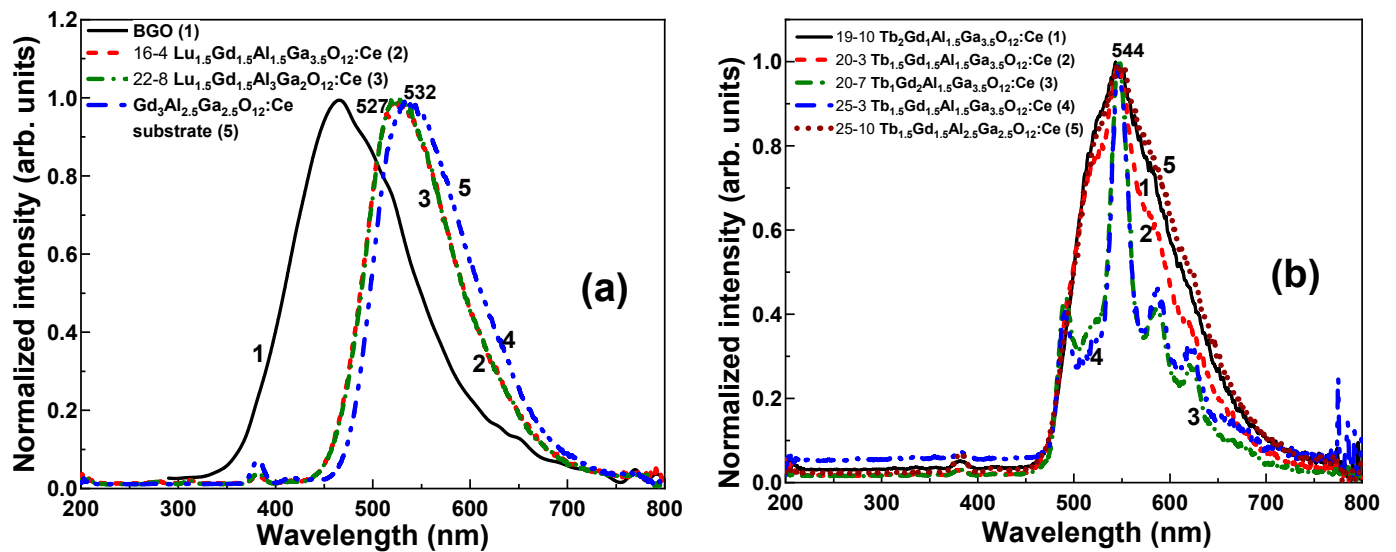


Figure 6. (a) Normalized XRL spectra of the selected Lu-Gd- (a) and Tb-Gd-based (b) composite scintillators in comparison with GAGG:Ce substrate and reference BGO scintillator.

Table 3. Scintillation yield parameters of the selected composite scintillators.

Sample	LY ^{241}Am at 1 μs and 10 μs (ph/MeV)	LY Difference between 0.5 and 10 μs of Shaping Time (%)	LY ^{137}Cs at 1 μs and 10 μs (ph/MeV)	LY Difference between 0.5 and 10 μs of Shaping Time (%)	LY(γ -rays)/LY(α -rays) at 1 μs
GAGG:Ce substrate	5084–5314	23.0	38,500–41,352	20.0	7.6
PL 16-4 $\text{Lu}_{1.5}\text{Gd}_{1.5}\text{Al}_{1.5}\text{Ga}_{3.5}\text{O}_{12}:\text{Ce}/\text{GAGG}:\text{Ce}$	1224–1607	53.1	36,873–39,202	19.2	30
PL 19-10 $\text{Tb}_2\text{GdAl}_{1.5}\text{Ga}_{3.5}\text{O}_{12}:\text{Ce}/\text{GAGG}:\text{Ce}$	110–281	284.9	32,269–34,728	21.2	293
PL 20-3 $\text{Tb}_{1.5}\text{Gd}_{1.5}\text{Al}_{1.5}\text{Ga}_{3.5}\text{O}_{12}:\text{Ce}/\text{GAGG}:\text{Ce}$	167–272	147.8	33,530–35,057	23.9	201
PL 20-7 $\text{Tb}_1\text{Gd}_2\text{Al}_{1.5}\text{Ga}_{3.5}\text{O}_{12}:\text{Ce}/\text{GAGG}:\text{Ce}$	80–182	169.3	31700–33,759	22.5	398
PL 22-8 $\text{Lu}_{1.5}\text{Gd}_{1.5}\text{Al}_3\text{Ga}_2\text{O}_{12}:\text{Ce}/\text{GAGG}:\text{Ce}$	2103–2720	53.1	32,946–35,619	20.4	15.65
PL 25-3 $\text{Tb}_{1.5}\text{Gd}_{1.5}\text{Al}_{1.5}\text{Ga}_{3.5}\text{O}_{12}:\text{Ce}/\text{GAGG}:\text{Ce}$	244–263	19.2	31,718–32,139	16.1	130
PL 25-10 $\text{Tb}_{1.5}\text{Gd}_{1.5}\text{Al}_2\text{Ga}_3\text{O}_{12}:\text{Ce}/\text{GAGG}:\text{Ce}$	245–254	17.8	31,334–31,758	15.3	128

The pulse-height spectra of GAGG:Ce substrate under α -particle and γ -quantum excitations measured at different shaping times are presented in Figure 7, while the dependences of light yield (LY) on shaping time for some studied composite scintillators are displayed in Figure 8. LYs under α -particle and γ -ray excitation are summarized in Table 3. The measured ratio of the LY under γ -ray and α -particle excitation was about 7.6, and this value is quite consistent with the data of [7].

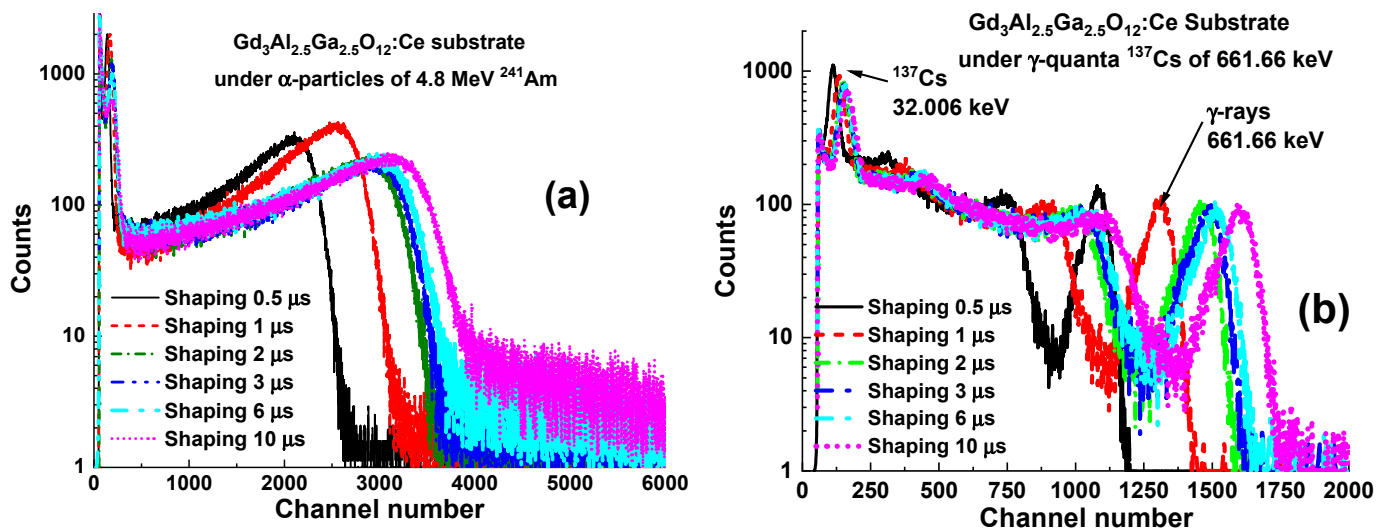


Figure 7. Pulse-height spectra of GAGG:Ce substrate under α -particle (a) and γ -quantum (b) excitation measured at different shaping times.

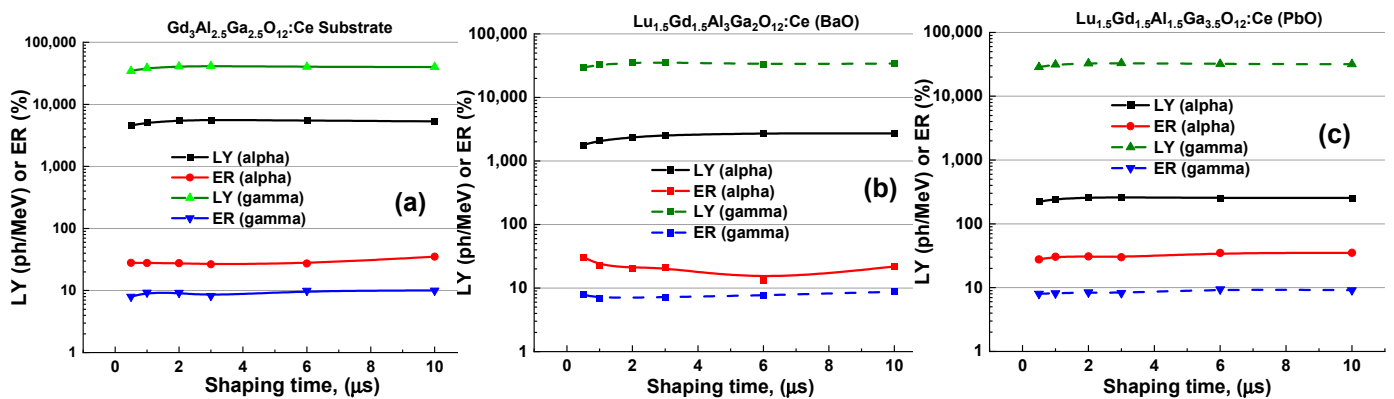


Figure 8. Dependences of LY and energy resolution (ER) of the GAGG:Ce substrates (a) and $\text{Gd}_{1.5}\text{Lu}_{1.5}\text{Al}_{1.5}\text{Ga}_{3.5}\text{O}_{12}:\text{Ce}$ / GAGG:Ce composite scintillators grown from BaO- (b) and PbO-based (c) fluxes, respectively, as the function of shaping time measured under various γ -rays of ^{137}Cs and α -particles of 4.8 MeV ^{241}Am (CERN ^{241}Am alpha source).

The LYs of the composite scintillators under γ -ray excitation were just a few thousand ph/MeV less than that in the GAGG:Ce substrate, with a low contribution of “slow” light, as indicated by the small differences in their values at 0.5 and 10 μs shaping times. This means that in the case of composite scintillators, γ -rays excite mainly the substrate scintillators and the contribution of light coming from the thin-film scintillators is insignificant.

The smallest contributions of “slow” light both under α - and γ -rays from 15.3 to 19.2% were registered in Tb-Gd garnet films grown from BaO flux, while the luminescence decay was remarkably slower in the rest of thin films. Specifically, the highest contribution of the slow luminescence components was registered in Gd-Tb garnet films grown from PbO flux.

The highest LY under α -particle excitation was registered in Lu-Gd garnet films, reaching 2720 ph/MeV, or $\sim 6\%$ of the light yield under γ -rays. However, the LYs of Tb-Gd garnet films were significantly (8–10 times) lower in comparison with those of their Lu-Gd counterparts. The LYs of Tb-Gd and Lu-Gd garnet films grown from BaO-based flux were 2–3 times higher than those of their analogs grown from PbO-based flux (Table 3), evidencing a negative role of Pb admixture in the scintillation process.

The timing characteristics of the selected composite scintillators are summarized in Table 4, where the rate of scintillation decay is characterized by the parameters $\tau_{1/e}$,

$\tau_{1/10}$, and $\tau_{1/100}$, representing the time of the signal attenuation until the 1/e, 10%, and 1% levels of the initial signal. Some types of composite scintillators demonstrated faster scintillation decay under γ -rays than under α - and β -particles; in contrast, others displayed the opposite trend. Such phenomena are related to the distribution of ionization density in an ionizing particle track (see [37,38] and related articles) and is outside the scope of this paper. Interestingly, GAGG:Ce film demonstrated faster scintillation decay under γ -rays, while in a GAGG:Ce film/GAGG:Ce crystal composite, the ratio was the opposite [7]. In our samples, the decay under γ -rays was the fastest among all the irradiation types in the initial part of the curve, and the slowest in the final part. Overall, the fastest decay and the largest $\tau_{\gamma}/\tau_{\alpha}$ and $\tau_{\gamma}/\tau_{\beta}$ ratios were registered in composites involving Lu-Gd mixed films (see the example of the $\text{Lu}_{1.5}\text{Gd}_{1.5}\text{Al}_3\text{Ga}_2\text{O}_{12}$:Ce SCF/GAGG:Ce SC sample shown in Figure 9).

Table 4. Scintillation decay parameters of $(\text{Gd,Lu,Tb})_3(\text{Al,Ga})_5\text{O}_{12}$:Ce SCF / GAGG:Ce SC composite scintillators under different types of excitation. A dash indicates no registered attenuation at this level within the 8000 ns measurement range.

	α -Particle Excitation by ^{239}Pu Source			β -Particle Excitation by ^{90}Sr Source			γ -Quantum Excitation by ^{137}Cs Source		
	$\tau_{1/e}$	$\tau_{1/10}$	$\tau_{1/100}$	$\tau_{1/e}$	$\tau_{1/10}$	$\tau_{1/100}$	$\tau_{1/e}$	$\tau_{1/10}$	$\tau_{1/100}$
GAGG:Ce Substrate	373	992	-	409	1058	-	300	899	-
PL16-4 $\text{Gd}_{1.5}\text{Lu}_{1.5}\text{Al}_{1.5}\text{Ga}_{3.5}\text{O}_{12}$:Ce SCF	124	630	6570	316	890	2930	245	785	2930
PL 20-7 $\text{Tb}_1\text{Gd}_2\text{Ga}_{3.5}\text{Al}_{1.5}\text{O}_{12}$:Ce SCF	441	1054	4130	370	952	3880	300	847	3260
PL 20-3 $\text{Lu}_{1.5}\text{Gd}_{1.5}\text{Al}_3\text{Ga}_2\text{O}_{12}$:Ce SCF	119	493	7090	290	854	~3100	263	799	~3100
PL 20-7 $\text{Tb}_2\text{GdAl}_{1.5}\text{Ga}_{3.5}\text{O}_{12}$:Ce SCF	434	1230	-	345	988	-	260	860	-
PL 22-8 $\text{Tb}_{1.5}\text{Gd}_{1.5}\text{Al}_{1.5}\text{Ga}_{3.5}\text{O}_{12}$:Ce SCF	422	1207	-	341	1002	-	265	910	-
PL 25-3 $\text{Tb}_{1.5}\text{Gd}_{1.5}\text{Al}_{1.5}\text{Ga}_{3.5}\text{O}_{12}$:Ce SCF	455	~2230	-	336	~2230	-	306	~2230	-
PL 25-10 $\text{Tb}_{1.5}\text{Gd}_{1.5}\text{Al}_2\text{Ga}_3\text{O}_{12}$:Ce SCF	359	915	-	257	778	-	242	721	-

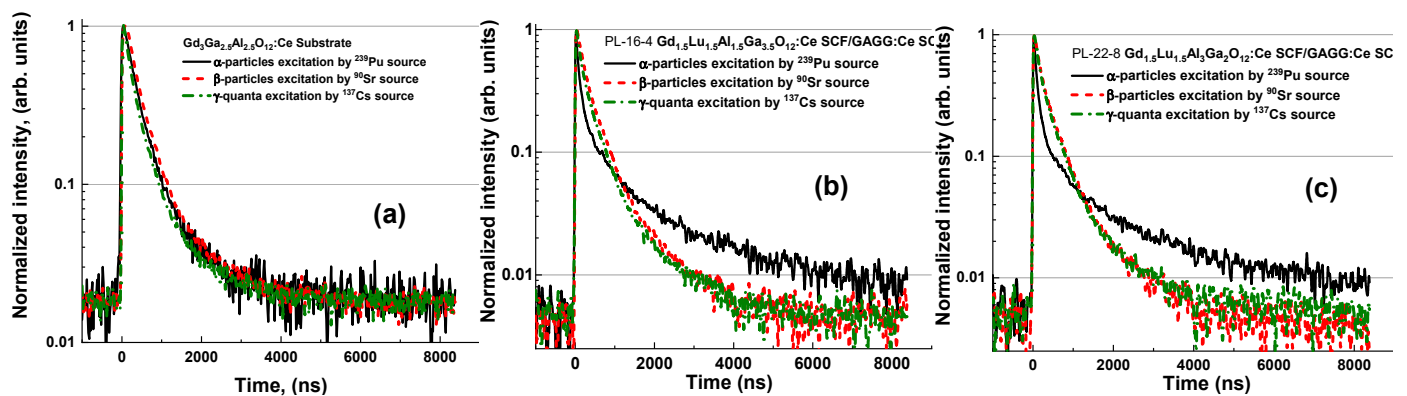


Figure 9. Scintillation decay of GAGG:Ce SC substrate (a) and $\text{Lu}_{1.5}\text{Gd}_{1.5}\text{Al}_{1.5}\text{Ga}_{3.5}\text{O}_{12}$:Ce SCF/GAGG:Ce SC composite scintillators grown from PbO- (b) and BaO-based (c) fluxes under α - and β -particle and γ -ray excitations.

Meanwhile, composite scintillators based on the Gd-Lu- and Gd-Tb-containing films demonstrated quite different scintillation decay behaviors in registration of different types of particles. In the Gd-Lu garnets, both γ -rays and β -particles were well distinguished from α -particles by scintillation timing (Figure 10a,b). The scintillation decay under α -particles was ~2.5 times faster within first few hundred ns, while it abruptly slowed down over longer times (Figure 9a,b). Herein, $\tau_{\alpha}/\tau_{\gamma}$ (a) and $\tau_{\alpha}/\tau_{\beta}$ (b) ratios sharply changed from 0.4–0.5 at the signal decay level of 1/e to 2.3 at the signal decay level of 1/100. The scintillation decay in Gd-Tb films was significantly slower compared to that in Lu-Tb films, and the $\tau_{\alpha}/\tau_{\gamma}$ and $\tau_{\alpha}/\tau_{\beta}$ ratios were within the ranges of 1–1.7 and 1–1.4, respectively.

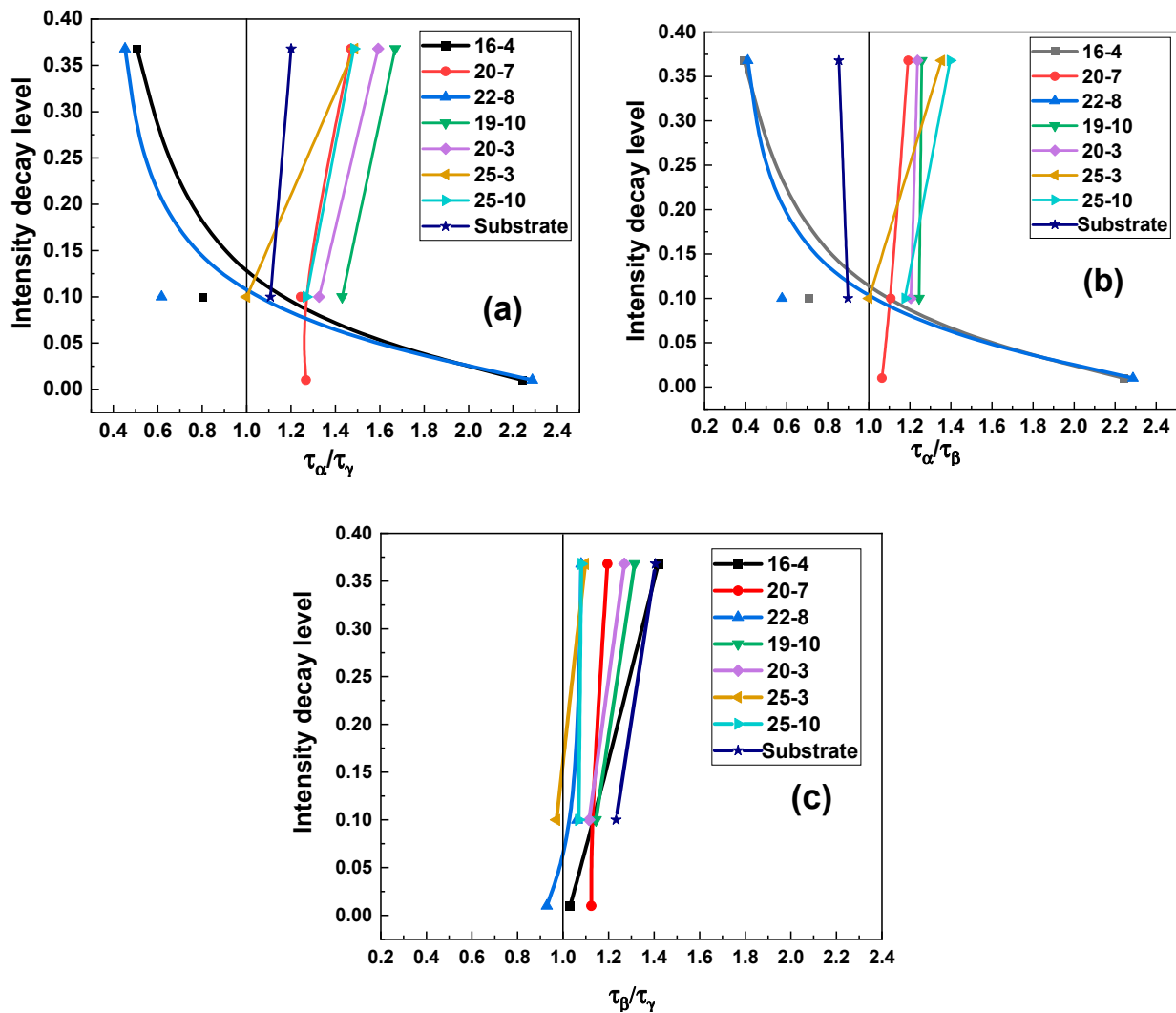


Figure 10. τ_α/τ_γ (a), τ_α/τ_β (b), and τ_β/τ_γ (c) ratios of the selected multicomponent composite scintillators under study (see Table 4 for the sample denotations).

The γ -rays and β -particles were rather poorly distinguished by scintillation timing in the composite scintillators under study (Figure 10c). A more remarkable difference was noted in the initial stage of scintillation decay for the intensity decay level of $1/e$, whereas at longer times the τ_β/τ_γ tended to 1 in most of the samples. Meanwhile, the best γ/β separation was demonstrated in composite scintillators based on Tb-Gd films ((Figures 10c and 11). Namely, in $\text{Tb}_{2-1.5}\text{Gd}_{1-1.5}\text{Al}_{1.5}\text{Ga}_{3.5}\text{O}_{12}:\text{Ce}$ SCF / GAGG:Ce SC composite scintillators the τ_β/τ_γ ratio reached 1.32 (Figure 10c).

Another figure of merit (FOM) parameter based on the normalized difference between the decay constants may better reflect the practical feasibility of the time discrimination of different types of particles using substrate-film scintillators, as compared with the case when using decay time ratios. This FOM is proportional not to the ratio between decay constants but to the difference between them—for example, for α - and β -particles it is expressed by Equation (1). Therefore, it is convenient to quantify the efficiency of distinguishing the particles and quanta using a FOM which equals 0 in the case of no discrimination and 1 in the case of ideal discrimination.

$$FOM_{\alpha\beta} = \frac{|\tau_\alpha - \tau_\beta|}{(\tau_\alpha + \tau_\beta)} \quad (1)$$

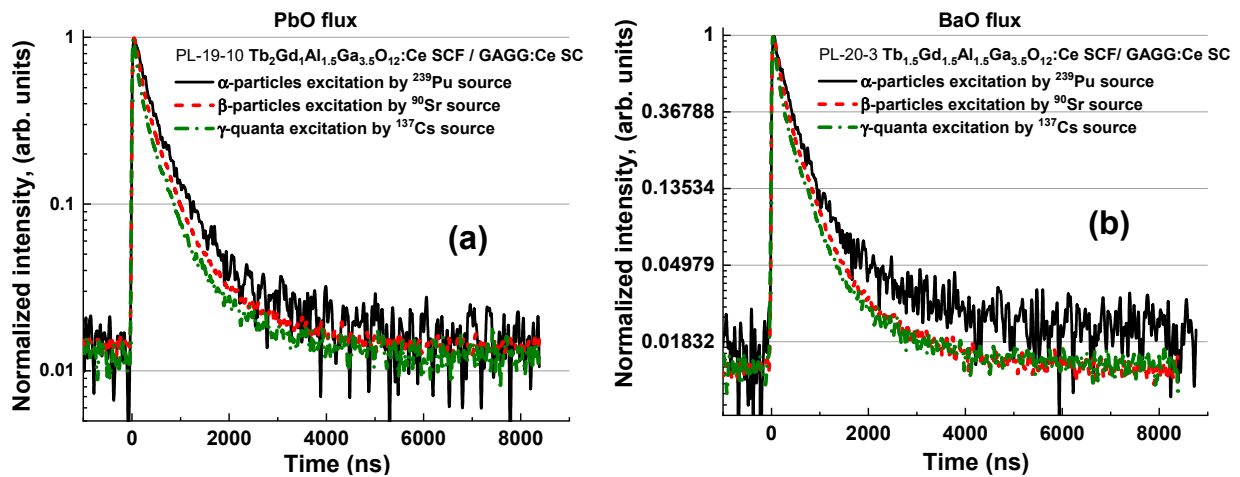


Figure 11. Scintillation decay of $\text{Tb}_2\text{Gd}_1\text{Al}_{1.5}\text{Ga}_{3.5}\text{O}_{12}:\text{Ce}$ SCF/GAGG:Ce SC (a) and $\text{Tb}_{1.5}\text{Gd}_{1.5}\text{Al}_{1.5}\text{Ga}_{3.5}\text{O}_{12}:\text{Ce}$ SCF/GAGG:Ce SC (b) composite scintillators grown from PbO- (a) and BaO-based fluxes, respectively, under α - and β -particle and γ -ray excitations.

The results presented in Figure 12 demonstrate that the highest $\text{FOM}_{\alpha\gamma}$ of up to 0.38 and highest $\text{FOM}_{\alpha\beta}$ of up to 0.44 were obtained with the $\text{Lu}_{1.5}\text{Gd}_{1.5}$ -substituted films, which seem promising for these discrimination tasks. $\text{FOM}_{\beta\gamma}$ did not exceed 0.13 (the highest value was again registered in the Tb_2Gd -substituted films).

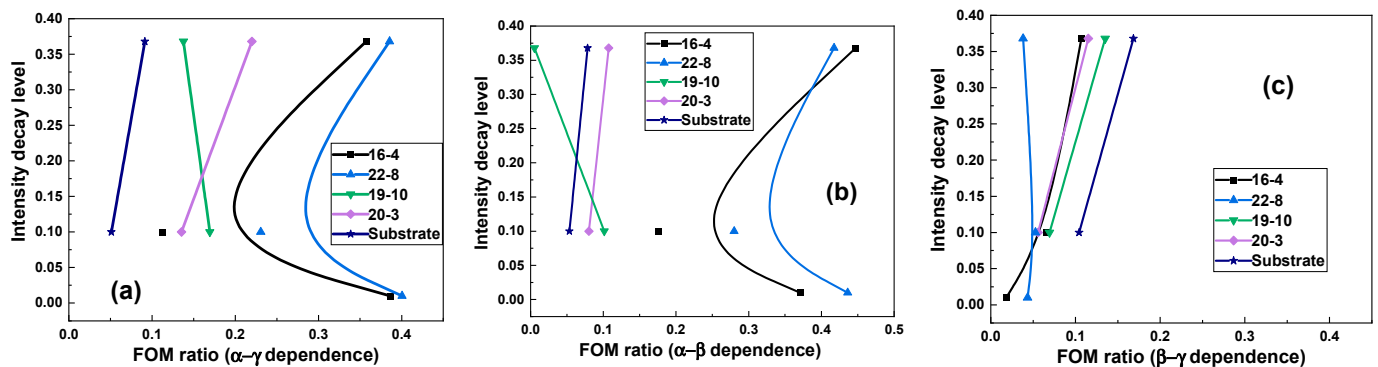


Figure 12. Figures of merit for the different pairs of irradiation types, $\text{FOM}_{\alpha\gamma}$ (a), $\text{FOM}_{\alpha\beta}$ (b), and $\text{FOM}_{\beta\gamma}$ (c) of the selected composite scintillators under study.

4. Discussion

With the goal of distinguishing the different components of radiation fluxes by scintillation decay dynamics, τ_α/τ_γ ratios were previously registered under the same experimental procedure in several garnet composite scintillators [8–10,12–14]. Obviously, the highest τ_α/τ_γ ratios were achieved in a system where substrate and film were doped with different activators. For example, they reached 16 in a $\text{LuAG}:\text{Pr}$ SCF/ $\text{LuAG}:\text{Sc}$ SC composite [10] and 6 in a $\text{Lu}_{3-x}\text{Tb}_x\text{Al}_5\text{O}_{12}:\text{Ce}$ SCF/ $\text{LuAG}:\text{Pr}$ SC scintillator [12]. The τ_α/τ_γ ratios in the systems where both substrate and film were doped with the same activator are remarkably lower, although the former were more convenient from a practical point of view as the responses from both the film and substrate could be registered by the same photodetector with the same efficiency. In particular, in GAGG:Ce SCF/GAGG:Ce SC composites with varying Al/Ga ratios, this parameter was within the range of 1.18–1.50 [13,14].

The results for Gd-Tb-substituted films on GAGG:Ce substrates in the present work, in general, repeat these values. Meanwhile, the scintillation decay in Lu-Gd-substituted systems demonstrated a completely different trend where the decay under α -particles is faster than that under γ -rays in the time range up to approximately 1000 ns, and slower at

longer times. Herein, the τ_α/τ_γ and τ_a/τ_β ratios changed from 0.4 to 2.3. A similar trend with a low τ_α/τ_γ in the initial stage of scintillation decay and then its rapid increase was observed in a LuAG:Ce single crystal [8,9].

Another evaluation of the efficiency of signal discrimination by the scintillation decay kinetic under α - and β -particles and γ -quanta was performed using the respective FOMs (Figure 11). The highest FOM $_{\alpha\gamma}$ and FOM $_{\alpha\beta}$ were obtained with the Lu_{1.5}Gd_{1.5}-substituted films, which are more promising materials for α/γ and α/β discrimination in comparison with Tb_{2-1.5}Gd_{1-1.5}-based films.

Accounting for the highest light yield under α -particles registered in Lu_{1.5}Gd_{1.5}Al_{1.5-3}Ga_{3.5-2}O₁₂:Ce SCF/GAGG:Ce SC and overall faster decay as compared to Gd-Tb-substituted films, these composite scintillators seem to be the most promising for distinguishing α/γ - or α/β -particles via the character of scintillation decay. Meanwhile, scintillation decays under γ - and β -quanta were poorly distinguishable by all these types of composite scintillators. However, for Gd-Tb-substituted films the τ_β/τ_γ and FOM $_{\beta\gamma}$ values were notably better than those for the Gd-Lu counterpart (Figures 10 and 11). The τ_β/τ_γ and FOM $_{\beta\gamma}$ parameters may be improved in multilayer composite scintillators involving a substrate and a combination of two or more different Lu-Gd- and Gd-Tb-containing films responsible for the registration of different types of ionizing particles. This is a topic of further research.

5. Conclusions

(Lu,Gd,Tb)₃(Al,Ga)₅O₁₂:Ce film/Gd₃(Al,Ga)₅O₁₂:Ce crystal composite scintillators demonstrated a good performance at distinguishing α -particles from β -particles and γ -quanta in mixed radiation fluxes. Composite scintillators involving Gd-Lu- or Gd-Tb-substituted garnet films possessed a high light yield of 31,000–39,000 phot/MeV under γ -quantum excitation, whereas a high light yield of up to 2720 ph/MeV under α -particles was registered only in Lu-Gd-substituted films. Lu_{1.5}Gd_{1.5}Al_{3-1.5}Ga_{2-3.5}O₁₂:Ce SCFs/GAGG:Ce SC composite scintillators demonstrated remarkably faster scintillation decay under α -particle excitation, providing τ_α/τ_γ and τ_a/τ_β ratios ranging from 0.4 to 2.3, depending on the stage of the scintillation process. This unusual behavior of scintillation decay, namely a faster decay under α -particles in first 1000 ns of scintillation decay, should be studied in more detail in further work. Meanwhile, β -particles and γ -quanta were barely distinguished by the considered types of composite scintillators, and the highest τ_β/τ_γ ratio of 1.32 was achieved in Tb_{2-1.5}Gd_{1-1.5}Al_{1.5}Ga_{3.5}O₁₂:Ce SCF/GAGG:Ce SC composite scintillators. The calculated FOMs confirm rather good α - γ (0.38) and β - γ (0.44) discrimination, whereas the FOM in the case of beta-gamma discrimination was relatively low (0.13).

Overall, this work contributes to the development of scintillation detectors for monitoring dangerous radionuclides in mixed radiation fluxes consisting of different types of particles and quanta, which have different impacts on human health and environmental security. Such detectors should provide more reliable determination of different types of radiation for environmental security and medical diagnostics. These thin-film scintillators can also be used as visualization screens for radiation introscopy for different types of radiation with an extremely high spatial resolution of <1 μ m.

Author Contributions: O.S. writing—original draft preparation, data curation; writing—review and editing; D.K., I.G., A.F., V.G., T.Z., Y.S., S.W.-L., J.A.M., R.K.—investigation; M.N.—validation, editing, Y.Z.—conceptualization, methodology, validation, review and editing. All authors have read and agreed to the published version of the manuscript.

Funding: This work was performed in the frame of Polish NCN 2018/31/B/ST8/03390 project. O. Sidletskiy acknowledges the scholarship of the Polish National Agency for Academic Exchange under agreement No. PPN/ULM/2020/1/00298/U/00001. Partial support of the Czech Ministry of Education, Youth and Sports under Project SOLID21 CZ.02.1. 01/0.0/0.0/16_019/0000760 and Czech Science Foundation project GA21-17731S is acknowledged with thanks.

Data Availability Statement: Not applicable.

Conflicts of Interest: The authors declare no conflict of interest.

References

1. Zaitseva, N.; Rupert, B.L.; Pawelczak, I.; Glenn, A.; Martinez, P.H.; Carman, L.; Faust, M.; Cherepy, N.; Payne, S. Plastic scintillators with efficient neutron/gamma pulse shape discrimination. *Nucl. Instrum. Methods Phys. Res. A* **2012**, *688*, 88–93. [[CrossRef](#)]
2. Sénoville, M.; Delaunay, F.; Pârlog, M.; Achouri, N.L.; Orr, N.A. Neutron-gamma discrimination with organic scintillators: Intrinsic pulse shape and light yield contributions. *Nucl. Instrum. Meth. Phys. Res. A* **2020**, *971*, 164080. [[CrossRef](#)]
3. Zorenko, Y.; Novosad, S.S.; Pashkovskii, M.V.; Lyskovich, A.B.; Savitskii, V.G.; Batenchuk, M.M.; Malyutenkov, P.S.; Patsagan, N.I.; Nazar, I.V.; Gorbenko, V.I. Epitaxial structures of garnets as scintillation detectors of ionizing radiation. *J. Appl. Spectrosc.* **1990**, *52*, 645–649. [[CrossRef](#)]
4. Zorenko, Y.; Batenchuk, M.; Gorbenko, V.; Pashkovsky, M. Single-crystalline oxide films of the $\text{Al}_2\text{O}_3\text{-Y}_2\text{O}_3\text{-R}_2\text{O}_3$ system as optical sensors of various types of ionizing radiation: Significant advantages over volume analogs. *Proc. SPIE* **1997**, *2967*, 101. [[CrossRef](#)]
5. Globus, M.; Grinyov, B.; Ratner, M.; Tarasov, V.; Lyubinskiy, V.; Vydai, Y.; Ananenkov, A.; Zorenko, Y.; Gorbenko, V.; Konstankevych, I. New type of scintillation detectors for biological, medical, and radiation monitoring applications. *IEEE Trans. Nucl. Sci.* **2004**, *51*, 1297–1303. [[CrossRef](#)]
6. Zorenko, Y.; Gorbenko, V. Growth peculiarities of the $\text{R}_3\text{Al}_5\text{O}_{12}$ (R = Lu, Yb, Tb, Eu–Y) single crystalline film phosphors by liquid phase epitaxy. *Radiat. Meas.* **2007**, *42*, 907–910. [[CrossRef](#)]
7. Witkiewicz-Lukaszek, S.; Gorbenko, V.; Zorenko, T.; Syrotych, Y.; Mares, J.A.; Nikl, M.; Sidletskiy, O.; Bilski, P.; Yoshikawa, A.; Zorenko, Y. Composite Detectors Based on Single-Crystalline Films and Single Crystals of Garnet Compounds. *Materials* **2022**, *15*, 1249. [[CrossRef](#)]
8. Witkiewicz-Lukaszek, S.; Gorbenko, V.; Zorenko, T.; Paprocki, K.; Sidletskiy, O.; Gerasymov, I.; Mares, J.A.; Kucerkova, R.; Nikl, M.; Zorenko, Y. Novel all-solid-state composite scintillators based on the epitaxial structures of LuAG garnet doped with Pr, Sc and Ce ions. *IEEE Trans. Nucl. Sci.* **2018**, *65*, 2114–2119. [[CrossRef](#)]
9. Witkiewicz-Lukaszek, S.; Gorbenko, V.; Zorenko, T.; Paprocki, K.; Sidletskiy, O.; Gerasymov, I.; Mares, J.A.; Kucerkova, R.; Nikl, M.; Zorenko, Y. Composite scintillators based on the crystals and single crystalline films of LuAG garnet doped with Ce^{3+} , Pr^{3+} and Sc^{3+} ions. *Opt. Mater.* **2018**, *84*, 593–599. [[CrossRef](#)]
10. Witkiewicz-Lukaszek, S.; Gorbenko, V.; Zorenko, T.; Sidletskiy, O.; Arhipov, P.; Fedorov, A.; Mares, J.A.; Kucerkova, R.; Nikl, M.; Zorenko, Y. Liquid phase epitaxy growth of high-performance composite scintillators based on single crystalline films and crystals of LuAG. *CrystEngComm.* **2020**, *22*, 3713–3724. [[CrossRef](#)]
11. Gorbenko, V.; Witkiewicz-Lukaszek, S.; Zorenko, T.; Syrotych, Y.; Mares, J.A.; Kucerkova, R.; Nikl, M.; Sidletskiy, O.; Fedorov, A.; Zorenko, Y. Development of composite scintillators based on the LuAG:Pr single crystalline films FILMS and LuAG:Sc single crystals. *Crystals* **2021**, *11*, 846. [[CrossRef](#)]
12. Mares, J.A.; Witkiewicz-Lukaszek, S.; Gorbenko, V.; Zorenko, T.; Kucerkova, R.; Beitlerova, A.; D’Ambrosio, C.; Dlouhy, J.; Nikl, M.; Zorenko, Y. Alpha and gamma spectroscopy of Composite scintillators based on the LuAG:Pr crystals and single crystalline films of LuAG:Ce and (Lu,Gd,Tb)AG:Ce garnets. *Opt. Mater.* **2019**, *96*, 109268. [[CrossRef](#)]
13. Witkiewicz-Lukaszek, S.; Gorbenko, V.; Zorenko, T.; Sidletskiy, O.; Gerasymov, I.; Fedorov, A.; Yoshikawa, A.; Mares, J.A.; Nikl, M.; Zorenko, Y. Development of composite scintillators Based on single crystalline films and Crystals of Ce^{3+} -Doped (Lu,Gd) $_3$ (Al,Ga) $_5\text{O}_{12}$ Mixed Garnet Compounds. *Cryst. Growth Des.* **2018**, *18*, 1834–1842. [[CrossRef](#)]
14. Witkiewicz-Lukaszek, S.; Gorbenko, V.; Zorenko, T.; Syrotych, Y.; Kucerkova, R.; Mares, J.A.; Nikl, M.; Sidletskiy, O.; Fedorov, A.; Kurosawa, S.; et al. New types of composite scintillators based on the single crystalline films and crystals of $\text{Gd}_3(\text{Al,Ga})_5\text{O}_{12}:\text{Ce}$ mixed garnets. *Mater. Sci. Eng. B* **2021**, *264*, 114909. [[CrossRef](#)]
15. Witkiewicz-Lukaszek, S.; Gorbenko, V.; Zorenko, T.; Paprocki, K.; Sidletskiy, O.; Fedorov, A.; Kucerkova, R.; Mares, J.A.; Nikl, M.; Zorenko, Y. Epitaxial growth of composite scintillators based on $\text{Tb}_3\text{Al}_5\text{O}_{12}:\text{Ce}$ single crystalline films and $\text{Gd}_3\text{Al}_{2.5}\text{Ga}_{2.5}\text{O}_{12}:\text{Ce}$ crystal substrates. *CrystEngComm* **2018**, *20*, 3994–4002. [[CrossRef](#)]
16. Kamada, K.; Yanagida, T.; Pejchal, J.; Nikl, M. Scintillator-oriented combinatorial search in Ce-doped (Y,Gd) $_3$ (Ga,Al) $_5\text{O}_{12}$ multicomponent garnet compounds. *J. Phys. D Appl. Phys.* **2011**, *44*, 505104. [[CrossRef](#)]
17. Sidletskiy, O.; Kononets, V.; Lebbou, K.; Neicheva, S.; Voloshina, O.; Bondar, V.; Baumer, V.; Belikov, K.; Gektin, A.; Grinyov, B.; et al. Structure and scintillation yield of Ce-doped Al–Ga substituted yttrium garnet. *Mater. Res. Bull.* **2012**, *47*, 3249–3252. [[CrossRef](#)]
18. Philip, O.; Gunow, G.; Shestakova, I.; Berheide, M.; Durner, E.; Stoller, C.; Cherepy, N. Scintillation properties of single-crystal and ceramic GGAG(Ce) and ceramic GYGAG(Ce) at temperatures up to 200 °C. In Proceedings of the 2015 IEEE Nuclear Science Symposium and Medical Imaging Conference (NSS/MIC), San Diego, CA, USA, 31 October–7 November 2015; pp. 1–7. [[CrossRef](#)]
19. Korzhik, M.; Alenkov, V.; Buzanov, O.; Fedorov, A.; Dosovitskiy, G.; Grigorjeva, L.; Mechinsky, V.; Sokolov, P.; Tratsiak, Y.; Zolotarjovs, A.; et al. Nanoengineered $\text{Gd}_3\text{Al}_2\text{Ga}_3\text{O}_{12}$ scintillation materials with disordered garnet structure for novel detectors of ionizing radiation. *Cryst. Res. Technol.* **2019**, *54*, 1800172. [[CrossRef](#)]

20. Zorenko, Y.; Gorbenko, V.; Zorenko, T.; Sidletskiy, O.; Fedorov, A.; Bilski, P.; Twardak, A. High-performance Ce-doped multicomponent garnet single crystalline film scintillators. *Phys. Status Solidi RRL* **2015**, *9*, 489–4931. [[CrossRef](#)]
21. Zorenko, Y.; Nikl, M.; Gorbenko, V.; Savchyn, V.; Voznyak, T.; Kucerkova, R.; Sidletskiy, O.; Grynyov, B.; Fedorov, A. Growth and luminescent properties of Lu₂SiO₅ and Lu₂SiO₅:Ce single crystalline films. *Opt. Mater.* **2011**, *33*, 846–852. [[CrossRef](#)]
22. Zorenko, Y.; Gorbenko, V.; Savchyn, V.; Voznyak, T.; Gorbenko, V.V.; Nikl, M.; Mares, J.A.; Sidletskiy, O.; Grynyov, B.; Fedorov, A.; et al. Scintillation and luminescent properties of undoped and Ce³⁺ doped Y₂SiO₅ and Lu₂SiO₅ single crystalline films grown by LPE method. *Opt. Mater.* **2012**, *34*, 1969–1974. [[CrossRef](#)]
23. Zorenko, Y.; Gorbenko, V.; Zorenko, T.; Malinowski, P.; Jary, V.; Kucerkova, R.; Beitlerova, A.; Mares, J.A.; Nikl, M.; Fedorov, A. Luminescent and scintillation properties of Bi³⁺ doped Y₂SiO₅ and Lu₂SiO₅ single crystalline films. *J. Lum.* **2014**, *154*, 525–530. [[CrossRef](#)]
24. Kilian, A.; Bilski, P.; Gorbenko, V.; Zorenko, T.; Witkiewicz, S.; Paprocki, K.; Zorenko, Y. Thermoluminescent properties of cerium doped Lu₂SO₅ and Y₂SiO₅ single crystalline films grown from PbO-B₂O₃ and Bi₂O₃ fluxes. *Crystals* **2018**, *8*, 120. [[CrossRef](#)]
25. Zorenko, Y.; Gorbenko, V.; Konstankevych, I.; Voznyak, T.; Savchyn, V.; Nikl, M.; Mares, J.A.; Nejezchleb, K.; Mikhailin, V.; Kolobanov, V.; et al. Peculiarities of luminescence and scintillation properties of YAP:Ce and LuAP:Ce single crystals and single crystalline films. *Radiat. Meas.* **2007**, *42*, 528–532. [[CrossRef](#)]
26. Zorenko, Y.; Gorbenko, V.; Zorenko, T.; Voznyak, T.; Riva, F.; Douissard, P.A.; Martin, T.; Fedorov, A.; Suchocki, A.; Zhydachevski, Y. Growth and luminescent properties of single crystalline films of Ce³⁺ doped Pr_{1-x}LuxAlO₃ and Gd_{1-x}LuxAlO₃ perovskites. *J. Cryst. Growth* **2017**, *457*, 220–226. [[CrossRef](#)]
27. Riva, F.; Douissard, P.-A.; Martin, T.; Carla, F.; Zorenko, Y.V.; Dujardin, C. Epitaxial growth of gadolinium and lutetium-based aluminum perovskites thin film for X-rays micro-imaging applications. *CrystEngComm* **2016**, *18*, 608–615. [[CrossRef](#)]
28. Gorbenko, V.; Zorenko, T.; Paprocki, K.; Riva, F.; Douissard, P.A.; Martin, T.; Zhydachevskii, Y.; Suchocki, A.; Fedorov, A.; Zorenko, Y. Epitaxial growth of the single crystalline films scintillating screens based on the Eu³⁺ doped RAlO₃ (R = Y, Lu, Gd, Tb) perovskites. *CrystEngComm* **2018**, *20*, 937–945. [[CrossRef](#)]
29. Robertson, J.M. Liquid phase epitaxy of garnets. *J. Cryst. Growth* **1978**, *45*, 233–242. [[CrossRef](#)]
30. Van Erk, W.; Robertson, J.M. Segregation in liquid phase epitaxy of garnets. *J. Cryst. Growth* **1982**, *59*, 543–547. [[CrossRef](#)]
31. Fasoli, M.; Vedda, A.; Nikl, M.; Jiang, C.; Uberuaga, B.P.; Andersson, D.A.; McClellan, K.J.; Stanek, C.R. Band-gap engineering for removing shallow traps in rare-earth Lu₃Al₅O₁₂ garnet scintillators using Ga³⁺ doping. *Phys. Rev. B* **2011**, *84*, 081102. [[CrossRef](#)]
32. Dorenbos, P. Electronic structure engineering of lanthanide activated materials. *J. Mater. Chem.* **2012**, *22*, 22344. [[CrossRef](#)]
33. Dorenbos, P. Electronic structure and optical properties of the lanthanide activated RE₃(Al_{1-x}Ga_x)₅O₁₂ (RE = Gd, Y, Lu) garnet compounds. *J. Lum.* **2013**, *134*, 310–318. [[CrossRef](#)]
34. Song, Z.; Zhou, D.; Liu, Q. Tolerance factor and phase stability of the garnet structure. *Acta Cryst. C* **2019**, *75*, 1353. [[CrossRef](#)]
35. Song, Z.; Xia, Z.; Liu, Q. Insight into the Relationship between Crystal Structure and Crystal-Field Splitting of Ce³⁺ Doped Garnet Compounds. *J. Phys. Chem. C* **2018**, *122*, 3567. [[CrossRef](#)]
36. Gu, X.; He, Z.; Sun, X.Y.; Xu, L.-D.; Shi, M.-F. Preparation and luminescence properties of Tb³⁺-doped garnet Y₂Mg₂Al₂Si₂O₁₂ luminescent materials. *Luminescence* **2021**, *36*, 834–838. [[CrossRef](#)] [[PubMed](#)]
37. Gektin, A.V.; Vasil'ev, A.N. Fluctuations of ionizing particle track structure and energy resolution of scintillators. *Funct. Mater.* **2017**, *24*, 621–627. [[CrossRef](#)]
38. Belsky, A.; Lebbou, K.; Kononets, V.; Sidletskiy, O.; Gektin, A.; Auffray, E.; Spassky, D.; Vasil'ev, A.N. Mechanisms of luminescence decay in YAG-Ce,Mg fibers excited by γ- and X-rays. *Opt. Mater.* **2019**, *92*, 341–346. [[CrossRef](#)]